KSCE Journal of Civil Engineering (2016) 20(7):2746-2754
DOI 10.1007/s12205-016-0488-3

Geotechnical Engineering
pISSN 1226-7988, eISSN 1976-3808
www.springer.com/12205

Experimental and Theoretical Investigation on the Stability of Deep Excavations against Confined Aquifers in Shanghai, China

Yu-yong Sun*

Received June 25, 2015/Revised October 14, 2015/Accepted November 29, 2015/Published Online January 22, 2016

Abstract

Urban development often requires deep excavations, such as for deep basements, cut-and-cover tunnels, and underground transportation systems. Pressure from a confined aquifer can cause a sudden failure of a deep excavation and have disastrous effects on the surrounding buildings. In this study, a series of centrifugal model tests were conducted on different aquitards in Shanghai to investigate the failure process and types. Two types of failure were identified from the centrifugal model tests: local failure (sand piping and sand boiling) and general upheaval. An approach to the stability analysis of deep excavation against a confined aquifer was developed. To increase the reliability of the analytical approach, the calculated results were compared with the experimental results. The results showed good agreement.

Keywords: *deep excavation, stability against confined aquifer, centrifugal model test, local failure, general upheaval*

1. Introduction

With the large-scale development and utilization of urban underground space, deep excavations such as for deep basements, cut-and-cover tunnels, underground parking, and underground transportation systems are increasing. As excavation depths increase, the stability of deep excavations along coastal regions will be challenged by confined aquifers existing below the excavations. The failure of deep excavations under pressure from a confined aquifer usually causes significant damage to nearby buildings, such as large deformations and cracking of buildings, damage to underground pipelines, and collapsed roads (Chow *et al.*, 1999; Liu *et al.*, 2002; Li *et al.*, 2004). Deep excavations against a confined aquifer need to be evaluated for their stability. Although treatment methods and their effects have been investigated based on the type of the confined aquifer (Wang *et al.*, 2013; Zhang *et al.*, 2013), the Chinese, Japanese, and Taiwanese codes still use the Pressure Balance Method (PBM) as the only criterion for deep excavations against a confined aquifer (Ministry of Housing and Urban-Rural Development of the People's Republic of China (MOHURD), 2012; Japanese Society of Architecture (JSA), 1988; Taiwan Geotechnical Society (TGS), 2011). According to the PBM, an excavation will fail when the confined aquifer pressure is equal to the soil pressure above the confined aquifer. However, the types of failure caused by confined aquifers are unknown. In addition, the PBM neglects the shear strength of soils. Thus, its use in practical engineering is controversial.

Current studies regarding the stability of deep excavations affected by groundwater have focused on the seepage flow under sand conditions (e.g., Terzaghi, 1943; McName, 1949; Marsland, 1953; Tanaka *et al.*, 1999; Benmebarek *et al.*, 2005; Wudtke, 2008). Terzaghi (1943) first addressed the influence of seepage flow on the stability of retaining excavations. He used model tests to find that the failure shape of the sand column lifted by the water could be assumed to be a rectangular prism adjacent to the excavation wall. The safety factor against the bulk heave can be determined by the ratio of the submerged weight of the prism compared to the excess water force on the prism base. McName (1949) identified two types of seepage failure: local failure ("piping" or "boiling") and general upheaval ("heaving"). Marsland (1953) and Tanaka *et al.* (1999) studied the seepage failure of sand in strutted sheeted excavations by using model tests. Benmebarek et al. (2005) used the FLAC 2D code to analyze the failure of sandy soil within a cofferdam subjected to an upward seepage flow. For cohesive soil, model tests have been carried out to visualize the failure mechanism and identify the relevant failure type (Wudtke and Witt, 2006; Wudtke, 2008). While most of the literature has been focused on the failure of excavations caused by seepage flow around sheet piles or braced walls, Ding (2014) analyzed the influence of inducing factors such as the head, length, and width of the confined aquifer on the stability of deep excavations by using 3D finite element methods.

In Shanghai, there are two confined aquifers at a depth of 100 m from the surface: a gray sandy silt layer ⑤$_2$ and silty fine sand layer ⑦. In addition, there are two aquitards: a gray silt clay

*Associate Professor, College of Civil Engineering, Tongling University, Cuihu NO. 4 Road 1335 Tongling Anhui 244000, China (Corresponding Author, E-mail: sunyuyong2@126.com)

layer ④ and dark green silty clay layer ⑥ (SGMTEB, 1999; Xu *et al*., 2009, 2013). Deep excavations under the pressure of a confined aquifer still fail, and the failure mechanisms are still controversial. In this study, therefore, centrifugal model tests were performed to analyze the influence of aquitards on the confined aquifer head and failure mechanisms. Methodologies to analyze the stability of deep excavations against a confined aquifer were developed. The results calculated with these methods showed good agreement with the experimental results of the centrifugal model tests.

2. Centrifugal Model Testing

2.1 Equipment

Geotechnical centrifugal model testing is a widely accepted method in geotechnical engineering (e.g., Craig, 1989; Taylor, 1995; Wang, 2015). Centrifugal model testing provides inertial forces by rotating a small-scale model at a high acceleration level. This produces a stress field that corresponds to the stress a prototype would experience. The L-30 geotechnical centrifugal apparatus has a design capacity of 20 *g*-t and maximum model acceleration of 200 *g* in dynamic tests. A model container with a transparent polymethyl methacrylate (PMMA) panel on the front surface and with dimensions of 415 mm × 228 mm × 355 mm was used, as shown in Fig. 1. In order to vary the pressure of the confined aquifer during the test process, the container was separated into two parts by a PMMA panel with holes below 50 mm. The width of the water tank was 50 mm. The change in the confined aquifer pressure was measured as the height of the buoy on the water surface corresponding to the graduated scale attached to the container. The optimal centrifugal acceleration was 100 *g* considering the scale of deep excavations and ability to measure the deformation against the fact that a greater centrifugal acceleration increases the measurement accuracy. Based on the similarity theorem, the model size was only 1% of the field size.

2.2 Sample Preparation

Based on the geological structure of the Shanghai Administrative Region at the depths associated with deep excavations, the soil samples were divided into two groups: the aquitard ④ and confined aquifer ⑤$_2$ and the aquitard ⑥ and confined aquifer ⑦.

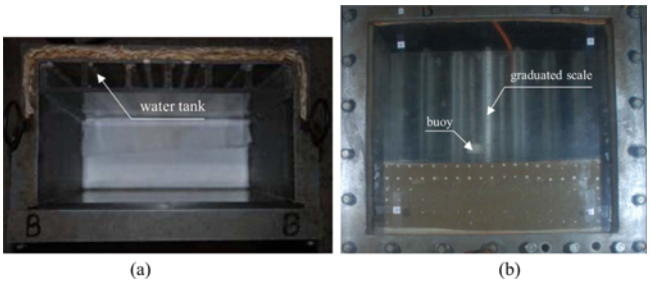

Fig. 1. View of Container with Water Level Controlling Equipment: (a) Top View, (b) Front View

Table 1. Material Properties of Soil

No.	Unit weight γ(kN/m^3)	Water content (%)	Void ratio	Consolidated quick shear	
				Cohesion (kPa)	Friction angle (^{o})
④	17.5	44.8	1.458	14	11
⑤$_2$	18.1	32.4	0.938	4	29
⑥	19.6	24.3	0.700	42	20
⑦$_2$	18.9	26.7	0.765	0	32.5

Table 1 presents the soil's mechanical properties. The thicknesses of the aquitard and confined aquifer in the model were 50 and 70 mm, respectively, while the actual thicknesses were 5.0 and 7.0 m, respectively.

As indicated in Table 1, the field water contents of layers ⑤$_2$, ⑥, and ⑦$_2$ were relatively low. Using the centrifuge to consolidate the soil samples was not possible; hence, the soil samples were prepared according to two alternative methods. For layer ④, the soil sample was first made into a paste with a water content of 80%-120% and then consolidated layer-by-layer with the centrifuge. Each layer had a thickness of 20-30 mm. The primary mechanical properties of each layer were the water content, unit weight, cohesion, and the internal friction angle. For layers ⑤$_2$, ⑥, and ⑦$_2$, the samples were dried, crushed, and sieved where the diameter of the sieve pores was 1 mm. The samples were then measured for water content, made into soil pastes based on the onsite water content, and finally tamped layer-by-layer based on the onsite unit weight.

In order to prevent water inrushing between the soil and sidewall of the container, the surface of the PMMA panel and sidewall of the container were first roughed with an abrasive paper or steel brush to enhance the frictional resistance. Second, waterproof silica gel was applied to the top surface of the confined aquifer. Finally, container movement was minimized to prevent the soil sample from being disturbed.

2.3 Simulating Confined Aquifer Pressure

The pressure of a confined aquifer was simulated by injecting water into the tank. A separate container on the centrifuge was the source of the injected water. The water injection volume was controlled with a bilateral switch on the water pipe that connected the water tank and container. The water tank was connected to the confined aquifer through the holes on the PMMA panel.

The pressure head was incremented to study the influence of the confined aquifer pressure on the stability of an excavation. The incremental sequence used until failure was 7, 10, 11, 12, and 13 cm corresponding to field dimensions of 7, 10, 11, 12, and 13 m, respectively. Each increment lasted 3 min. The corresponding real time can be calculated through the similarity theorem:

$$t_r = t_m \cdot N^2 = 3 \times 100^2 = 3 \times 10^4 (\text{min}) = \frac{3 \times 10^4}{60 \times 24} = 21(d) \quad (1)$$

where t_r is the real time (days), t_m is the model time (minutes),

Table 2. Experimental Results

NO.	Aquitards	Thickness (m)	Failure water pressure			Failure types
			PBM (kPa)	Experimental results (kPa)	Ratio (η)	
6-1	⑥	4.78	93.7	105	1.12	Sand piping at corner
6-2	⑥	4.82	94.5	125	1.32	Sand boiling
6-3	⑥	4.83	94.7	111	1.17	Sand piping at side
6-4	⑥	4.71	92.3	118	1.28	Sand boiling
6-5	⑥	4.74	92.9	121	1.30	General upheaval
6-6	⑥	5.56	110.1	142	1.29	Sand boiling
6-7	⑥	5.88	116.4	149	1.28	Sand boiling
4-1	④	4.79	83.8	102	1.21	General upheaval
4-2	④	4.95	86.6	114	1.32	Sand boiling
4-3	④	5.75	100.6	112	1.11	General upheaval
4-4	④	5.37	94.0	99	1.05	Sand piping at side
4-5	④	4.95	86.6	102	1.18	Sand piping at corner

and N is the centrifugal acceleration.

Based on Eq. (1), the real-time duration was 21 days for a test time of 3 min. Therefore, the water heads of the aquifer and water tank were equivalent, and the aquitard deformation was stable under these test conditions.

2.4 Testing Procedure

The testing procedure was as follows:

(1) Soil samples were prepared as presented above.
(2) The soil samples were reconsolidated to exclude soil settlement.
(3) Water was injected into the container on the centrifuge tumbler to simulate the pressure of a confined aquifer. The injected water volume could be calculated based the estimated water head at failure. A surplus volume of water should be considered.
(4) The model container was lifted into the centrifuge. The camera was positioned to record the failure process.
(5) The centrifuge was started and gradually accelerated to the design acceleration of 100 *g*.
(6) The confined aquifer pressure was applied incrementally as discussed above. Each increment was maintained for 3 min, and water was reinjected when the container level decreased. The stable aquitard was observed, and the failure process was observed while the centrifuge acceleration was maintained.
(7) Failure was confirmed when a large quantity of water rushed on top of the soil sample or when the water level rapidly decreased. At that point, the centrifuge was stopped, and the model container was removed.
(8) The failure characteristics were recorded, and the average thickness of the aquitard was measured.

3 Experimental Results and Discussion

3.1 Failure Types of Excavation Against a Confined Aquifer

Twelve centrifugal model tests were conducted to investigate the process and types of failure for a deep excavation against a confined aquifer. Based on the experimental results and experience in practice, two types of failures were identified: local failure (including sand piping and sand boiling) and general upheaval. These results are similar to the conclusions of McName (1949), Wudtke and Witt (2006), and Wudtke (2008). Table 2 presents the experimental results.

3.1.1 Local Failure

Based on the observed failure characteristics, local failure can

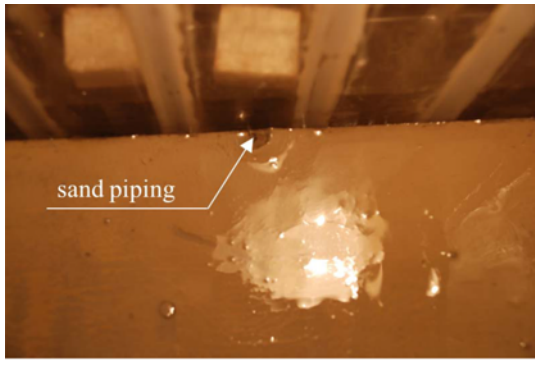

(a)

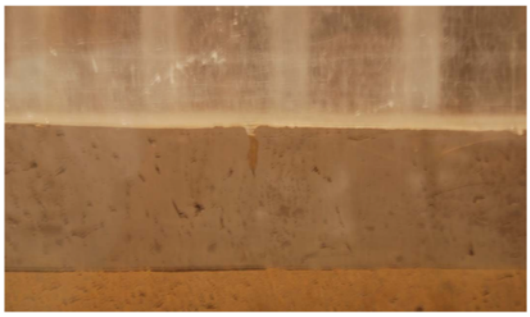

(b)

Fig. 2. Sand Piping at the Container-soil Interface: (a) Top View, (b) Front View

Fig. 3. Sand Piping at the Corner

be divided into two groups: sand piping and sand boiling.

3.1.1.1 Sand piping

When the confined aquifer pressure was increased to 1.05-1.32 times that of the soil pressure above the confined aquifer, the sand erupted around the container–soil interface onto the surface of the aquitard to form a small dune, as shown in Figs. 2 and 3. A channel for sand piping was formed in the aquitard, as shown in Fig. 2(b). Meanwhile, the water tank level decreased dramatically. This type of failure typically occurs at the interface between the wall of the model container/retaining structure and the soil. This failure mechanism can be controlled by blocking the channel or by ballasting, which reduces the adverse effects on the surrounding buildings and maintains the stability of the deep excavation itself. The confined aquifer pressure at failure is relatively small; the minimal ratio between the experimental value and the value calculated with the PBM (MOHURD, 2012) was 1.05. Thus, the stability of a deep excavation against sand piping should be confirmed first in stability calculations.

Sand piping is primarily caused by the lower contact strength and disturbance of piles or pipes in excavations (Chow *et al.*, 1999). These factors can be eliminated by improving the onsite construction quality and management techniques. The lateral compressing action of the retaining structure during excavation can also increase the contact strength. Therefore, measures to mitigate this failure type are not further discussed in the subsequent sections of this report.

3.1.1.2 Sand boiling

Figure 4 shows the failure characteristics of sand boiling, which occurred in five of the 12 tests. One or more cracks occur on the surface of the aquitard, which allows the sand within the confined aquifer to erupt from the cracks. This then causes a sudden decrease in the water tank level. This failure type has the characteristics of being instantaneous and without warning. Hence, serious damage is inevitable if this failure happens. In the experimental results, sand boiling commonly occurred in layer because this was a hard plastic soil and therefore prone to tensile damage.

Because a tensile stress will occur on the excavation bottom with a confined aquifer, a failure criterion for soil under a state of

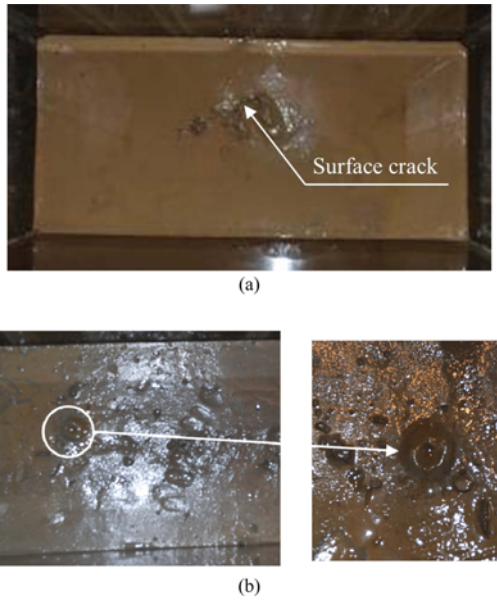

Fig. 4. Sand Boiling: (a) Sand Boiling from Surface Crack, (b) Sand Boiling from Surface Point

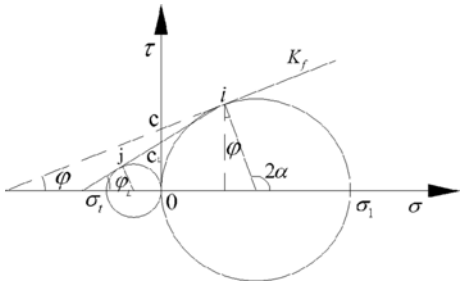

Fig. 5. Modified M-C Failure Envelope

low stress should be proposed. Based on testes, Sun (2011) proposed a failure criterion for soils with tensile stress that involves neither tension failure nor shear failure (Carter, 1986). Sun (2011) proposed the tensile-shear failure criterion to determine the stable state of soils under low stress. Fig. 5 shows the modified More-Coulomb failure envelope.

Based on the failure characteristics and failure criterion of soils under low stress (Sun, 2011), the mechanism for sand boiling failure can be described as follows. When $h < h_{cr}$, where h is the real thickness of the aquitard and h_{cr} is the critical thickness of the excavation failure according to the PBM (MOHURD, 2012; JSA, 1988; TGS, 2011), the uplift deformation of the aquitard is induced by the following upward pressure :

$$p = \gamma_w H_w - \gamma h \tag{2}$$

where γ_w is the unit weight of water, H_w is the confined aquifer head, γ is the unit weight of the aquitard, and h is the thickness of the aquitard

The uplift deformation in the middle of the aquitard is greater than that of the surroundings due to the constraining effects of the retaining structure. Meanwhile, the horizontal tensile stress of the surface soil develops as the water head rises. When the soil's

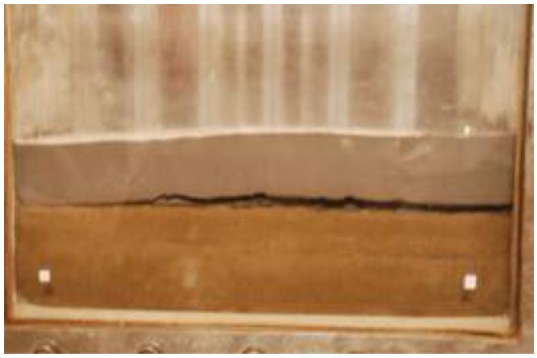

Fig. 6. General Upheaval

stress level reaches the tensile-shear failure criterion, tensile-shear failure occurs at the soil surface as indicated by the appearance of cracks. Subsequently, the effective thickness, stiffness, and shear strength of the aquitard are further weakened. This results in the expansion of the depth of the tensile-shear failure zone, which ultimately causes the confined aquifer to erupt from the penetrating passage.

3.1.2 General Upheaval

Figure 6 shows the failure characteristics of general upheaval, which occurred in three of the 12 tests. When the pressure of the confined aquifer increases to 1.11-1.30 times the soil pressure above the confined aquifer, the aquitard uplifts relative to the enclosed structure. The lateral deformation of the middle and bottom of the retaining structure increase as well. This failure type gradually evolves into an overall failure of the excavation site, which causes significant damage to the surrounding environment.

The mechanism of overall heaving is shear failure near the interface between the aquitard and retaining structure, similar to the direct shear test. However, the stress and strain fields are not constant because the model for the aquitard was based on a thickness and width of tens of meters. Due to the upward action of the confined aquifer, the stress and strain fields become more complicated, which results in the soil structure failing near the interface instead of at the interface.

3.2 Failure Confined Aquifer Pressure

The conclusions presented below were derived from the experimental results presented in Table 2.

(1) The safety of a deep excavation site is maintained when the confined aquifer pressure increases to the critical value as calculated by the BPM. The average failure confined aquifer pressure ratio η (i.e., the ratio between the experimental results and calculated value using the PBM) of layer ⑥ was 1.25, while that of layer ④ was 1.17.

(2) The experimental results showed that the failure confined aquifer pressure ratio η was about 1.30 for sand boiling, 1.05-1.20 for sand piping, and 1.10-1.30 for general upheaval. Therefore, sand piping occurs more often than general upheaval and sand boiling.

3.3 Size Effect of the Excavation on Failure

3.3.1 Test Profile

The size of a deep excavation has a significant influence on the stability of the excavated area. In order to study the size effect of an excavation on its failure, a laboratory model test was conducted in addition to the centrifugal model tests. The test equipment was the model container of the centrifuge. Layer ④ represented the aquitard and had a thickness of 50 mm, while layer $⑤_2$ represented the confined aquifer with a thickness of 70 mm. This test was conducted under gravity stress conditions. The plane size of the excavation was 415 mm × 178 mm, i.e. 1% of the size of the centrifugal model tests.

The testing procedure was as follows:

(1) The soil sample was prepared as described above.
(2) A dial indicator was installed, as shown in Fig. 7.
(3) The applied pressure at each test point due to the confined aquifer was incremented for 24 h.
(4) The deformation of the aquitard was measured, and the failure process was recorded.

3.3.2 Results and Analysis

The small-size model test showed that the size of a deep excavation has a distinct influence on the stability of an excavation against a confined aquifer. As shown in Fig. 8, when the confined aquifer head reached 15 cm (i.e., equal to 1.7 times

Fig. 7. Dial Gauge Installation Diagram

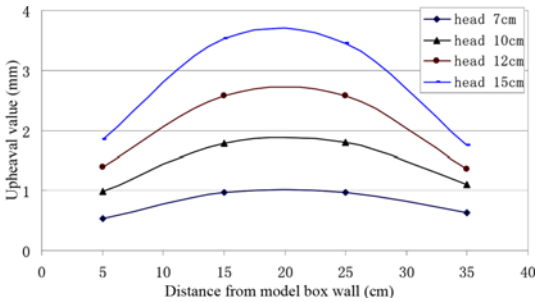

Fig. 8. Relationship between Uplift and Confined Water Pressure

the soil pressure above the confined aquifer), the maximum uplift deformation was only about 4 mm. Furthermore, failure did not occur. For reference, the maximum failure confined aquifer pressure ratio from the centrifugal model tests was 1.32.

4. Approach to Stability Analysis of an Excavation Against a Confined Aquifer

The yield criterion of soils under low stress is a controversial method; therefore, this approach is only used for general upheaval failures. In this study, numerical simulation and theoretical analysis were used for the stability analysis of an excavation against a confined aquifer.

4.1 Numerical Analysis

4.1.1 Numerical Modeling

The aim of this simulation was to determine the shape of the failure surface. Therefore, layer ⑥ was chosen in this study as a representative case. For the convenience of analysis, only the aquitard and retaining structure were included in the numerical model. The confined aquifer pressure was simplified as a uniform load. The hardening-soil model, which considers both shear hardening and compression hardening, was used to model the soil (Ducan *et al.*, 1970; Kondner *et al.*, 1963; PLAXIS, 2002). The failure criterion of the soil was based on the Mohr-Coulomb criterion. The 15-node triangular element is a very accurate element that leads to high-quality stress results and was used to model the soil layers. The interface elements were used to study the interaction between the soil and retaining structure. The interface element had zero thickness within the model. The bilinear model was used to represent the interface element, while the Mohr-Coulomb criterion (Yin *et al.*, 1995) was used to distinguish between the elastic and plastic behaviors. The strength properties of the interface were linked to the strength properties of the soil layer. These properties could only be determined by multiplying the soil strength parameters with a reduction factor (R_{inter}). Fig. 9 shows the meshed model. The aim of this simulation was to determine the shape of failure surface. Therefore, the following interface reduction factors were used: R_{inter} = 0.4, 0.5, 0.6, 0.7, 0.8, 0.9, and 1.0. The widths of the excavation used were 10, 12, 15, 17, 20, 30, 40, and 50 m, respectively. The retaining structure was simulated as a linear elastic plate. Tables 1 and 3 list the parameters of the simulation. The left and right vertical boundaries were restrained against both vertical and horizontal movements, while the top was a free surface. The pressure of the confined aquifer was applied to the bottom boundary as a uniform load.

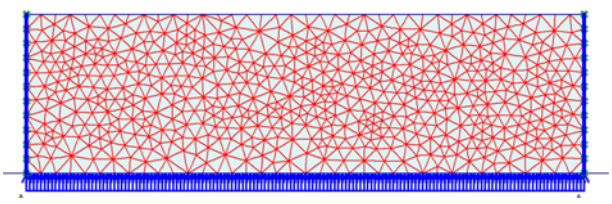

Fig. 9. The Meshed Model

Table 3. Parameters of simulation

Parameter	Value
Stress dependent stiffness according to a power law (m)	0.5
Plastic straining due to primary deviatoric loading (E_{50}^{ref}) (MPa)	45
Plastic straining due to primary compression (E_{oed}^{ref})/MPa	45
Elastic unloading/reloading (E_{ur}^{ref})/MPa	135
Poisson's ratio (v)	0.28

For safety, the yield and failure were considered equivalent in an idealized elastic-plasticity model. The failure of the deep excavation against a confined aquifer in the numerical simulation occurred when the plastic zone penetrated the aquitard.

4.1.2 Results and Discussion

Based on the calculated results, two types of failure zones occur because of the general upheaval failure mechanism. One zone is the contact surface between the soil and retaining structure ($R_{\text{inter}} < 0.8$), while the other zone is approximated by an arc in the soil adjacent to the deep excavation ($R_{\text{inter}} \geq 0.8$), as shown in Fig. 10. When the failure surface approximates an arc, the angle between the tangent of the arc failure surface and the horizontal plane is $45^{\circ} + \varphi/2 = 55^{\circ}$ (where φ is the internal friction angle of the aquitard). Fig. 11 shows the two types of failure zones.

Figure 12 shows the relationship between the critical confined

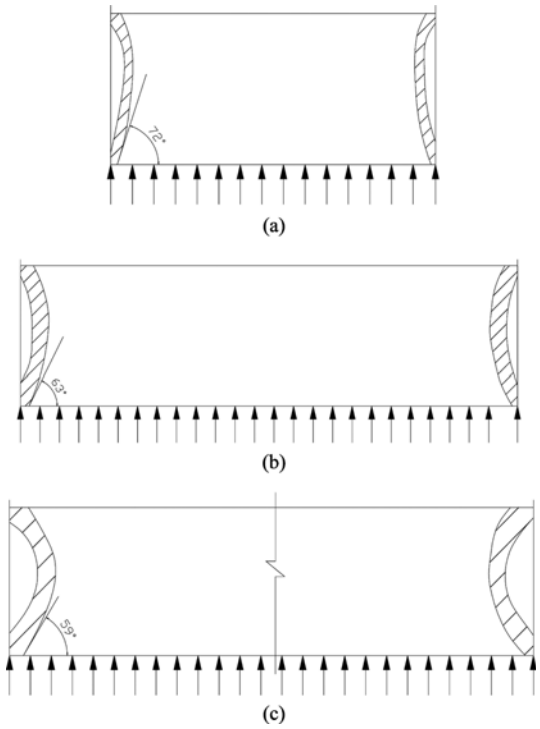

Fig. 10. The Failure Shape in the Failure Type of General Upheaval: (a) 10 m Width, (b) 17 m Width, (c) 40 m Width

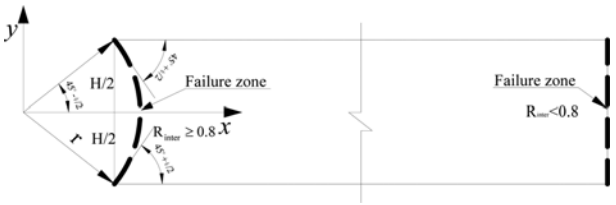

Fig. 11. Sketch of Failure Shape in the Failure Type of General Upheaval

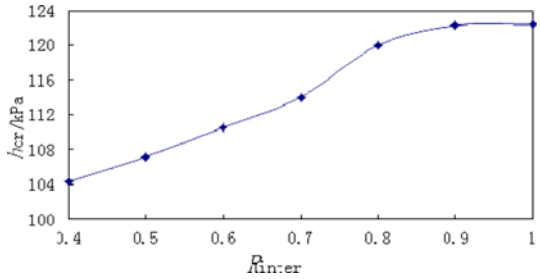

Fig. 12. Relationship between h_{cr} and R_{inter}

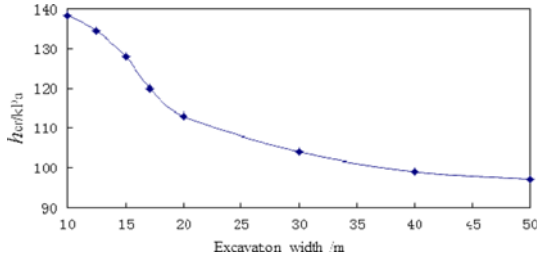

Fig. 13. Relationship between h_{cr} and Excavation Width

aquifer pressure (h_{cr}) when the excavation fails and the reduction factor of the contact surface strength (R_{inter}). The size of the aquitard was 41.5 m (L) ×17.8 m (W) ×4.73 m (H), and the soil was layer ⑥. When, $R_{inter} < 0.8$ h_{cr} increased linearly with R_{inter}. However, when $R_{inter} \geq 0.8$, then h_{cr} was approximately constant. This relationship indicates that neither the shear strength of the contact surface nor the failure zone at the contact surface is a decisive factor.

Figure 13 shows the relationship between h_{cr} and the width of the excavation when $R_{inter} = 0.9$. When the width of the excavation was less than 20 m and increasing, then h_{cr} quickly decreased. When the width of the excavation was greater than 20 m and increasing, h_{cr} gradually decreased and trended towards a fixed value. The results indicate that $h_{cr} = 97.1$ kPa when the width was 50 m. This value of h_{cr} can be considered equivalent to the soil pressure above the confined aquifer. Therefore, larger excavations can be concluded to have a higher potential for failure. Additionally, the PBM is the only way to evaluate the stability of an excavation against a confined aquifer as the width of the excavation increases. This further proves that the size effect is important to the stability of an excavation against a confined aquifer.

4.2 Evaluation Approach for General Upheaval

To establish an approach for evaluating an excavation against a confined aquifer for general upheaval failure, the shear resistance on the failure surface must first be derived. The shear resistance based on two types of failure zones can be calculated as follows.

The shear resistance can be determined from the shear strength of the interface area and the thickness of the aquitard when the failure zone is the interface between the soil and retaining structure.

The shear strength of the interface is given as follows:

$$\tau_{inter} = \gamma h K_0 \tan\varphi_{inter} + c_{inter} \tag{3}$$

where τ_{inter} is the shear strength of the interface, γ is the unit weight of the aquitard, h is the depth, K_0 is the static lateral pressure coefficient of the aquitard, c_{inter} is the interface cohesion, and φ_{inter} is the internal friction angle of the interfaces.

The shear resistance can be derived by integrating along the interface:

$$T = c_{inter} H + \int_0^H K_0 \gamma h \tan\varphi_{inter} dh = c_{inter} H + \frac{1}{2} K_0 \gamma H^2 \tan\varphi_{inter} \tag{4}$$

where T is the shear resistance on the failure surface and H is the thickness of aquitard.

When the failure zone is an arc, the arc radius can be calculated from the geometric relationship shown in Fig. 11:

$$r = \frac{H}{2\sin(45^\circ - \varphi/2)} \tag{5}$$

where r is the radius of the arc failure surface and φ is the internal friction angle of the aquitard.

The shear strength of the interface is given as follows:

$$\tau = \gamma h K_0 \tan\varphi + c \tag{6}$$

where c is the cohesion of the aquitard.

The shear resistance of the failure surface can be calculated by using the following formula:

$$T = cl + K_0 \gamma \tan\varphi \left[\int_{-(45^\circ - \varphi/2)}^{0} \left(\frac{H}{2} - r \sin\alpha \right) r \cos\alpha d\alpha + \int_0^{45^\circ - \varphi/2} \left(\frac{H}{2} + r \sin\alpha \right) r \cos\alpha d\alpha \right] = \frac{(90^\circ - \varphi)\pi Hc}{360^\circ \sin(45^\circ - \varphi/2)} + \frac{3}{4} H K_0 \gamma \tan\varphi \tag{7}$$

Table 4 compares the results of the numerical simulation and

Table 4. Comparison between Calculation and Numerical Simulation

R_{inter}	Failure confined water pressure (kPa)	
	Numerical simulation	Calculated
0.4	104.3	104.9
0.5	107.2	106.7
0.6	110.5	108.9
0.7	114.0	111.0
0.8	120.0	118.9
0.9	122.3	118.9
1.0	122.4	118.9

Table 5. Comparison between Calculated and Experimental Failure Confined Water Heads

NO.	Thickness (m)	Cohesion (kPa)	Friction angle (°)	Experimental value (m)	Calculated value (m)
6-5	4.74	42	20	12.1	11.22
4-1	4.79	14	11	10.2	9.5
4-3	5.75	14	11	11.2	10.8

the calculation using Eqs. (4) and (7). The difference between the simulated and calculated values was less than 5%, with the latter being more conservative.

The differences between the weight of the upward soil and the shear resistance between the soil and retaining structure were not overcome until general upheaval occurred. Considering the failure zones and excavation size, the approach can be represented as follows:

$$\frac{\gamma HS + CT}{\gamma_w H_w S} \geq K_v \tag{8}$$

where γ is the unit weight of the overlying soil, H is the thickness of the overlying soil, S is the plane area of excavation, C is the length around the excavation, T is the unit shear resistance between the soil and retaining structure as calculated with Eq. (4) or (7), H_W is the water head of the confined aquifer, and K_v is the safety factor of the excavation.

Table 5 compares the calculation based on Eq. (8) and the experimental failure of the confined aquifer head. A higher roughness of the contact area resulted in a failure surface that was assumed to be an arc. The calculated value was approximately equivalent to the experimental value and was more conservative.

5. Conclusions

In this work, a series of centrifugal tests and one model test were conducted to study the failure types and process for deep excavations under the effects of confined aquifer pressures in soft soils in Shanghai. The test results showed two failure types: local failure (sand piping and sand boiling) and general upheaval. Factors that influence the failure type are the characteristics of the aquitard, the plane size of excavation, and the contact shear strength between the soil and retaining structure. The size effect is distinct on the stability of an excavation against a confined aquifer. As discussed previously, a larger excavation has a higher potential for failure. There are two kinds of failure zones for general upheaval failures based on different contact strengths: the contact surface between the soil and retaining structure and the approximate arc surface near the contact surface. An approach to evaluating the types of general upheaval failure was proposed and discussed based on the theoretical analysis. The calculated results agreed with the experimental results.

Acknowledgements

The financial support received from the Anhui Provincial University Scientific Research Foundation (No. KJ2015A176), Anhui Provincial Natural Science Foundation (No. 1608085ME103) and Anhui Provincial Outstanding Young Talents Support Plan (No. gxyqZD2016308) are gratefully acknowledged.

References

Carter, J. P., Booker, J. R., and Yeung, S. K. (1986). "Cavity expansion in cohesive frictional soils." *Geotechnique*, Vol. 36, No. 3, pp. 349-358, DOI: 10.1680/geot.1986.36.3.349.

Chow, H. L. and Ou, C. Y. (1999). "Boiling failure and resumption of deep excavation." *Journal of Performance of Constructed Facilities*, Vol. 13, No. 3, pp. 114-120, DOI: 10.1061/(ASCE)0887-3828 (1999)13: 3(114).

Craig, W. H. (1989). "Edouard Phillips (1821-1889) and the idea of centrifuge modeling." *Geotechnique*, Vol. 39, No. 4, pp. 697-700, DOI: 10.1680/geot.1989.39.4.697.

Ding, C. L., Li, Z. Q., Wu, X. P., and Wu, K. L. (2014). "Analysis on inducing factors to inrushing plastic deformation failure of foundation pit with confined water." *Tunneling and Underground Construction*, pp. 491-500, DOI: 10.1061/9780784413449.048.

Duncan, J. M. and Chang, C. Y. (1970). "Nonlinear analysis of stress and strain in soil." *ASCE: Journal of the Soil Mechanics and Foundation Division*, No. 6, pp. 1629-1653.

Kondner, R. L. and Zelasko, J. S. (1963). "A hyperbolic stress-strain formulation for sand." *2nd Pan. Am. CSMFE*. Brazil, pp. 289-324.

Japanese Society of Architecture (JSA) (1988). *Guidelines of design and construction of deep excavation*, JSA, Tokyo.

Li, H. R. and Wu, S. M. (2004). "Treatments of Zhongyin building foundation pit bursting." *Exploration Engineering (Soil Drilling Engineering)*, No. 9, pp. 23-25. (in Chinese)

Liu, G. B. and Wang, H. X. (2002). "Influence of the pressure water in shallow silty sand in Shanghai on excavation." *Chinese Journal of Geotechnical Engineering*, Vol. 24, No. 6, pp. 790-792. (in Chinese)

Marsland, A. (1953). "Model experiments to study the influence of seepage on the stability of a sheeted excavation in sand." *Geotechnique*, Vol. 6, No. 3, pp. 223-241.

McNamee, J. (1949). "Seepage into a sheeted excavation." *Geotechnique*, Vol. 4, No. 1, pp. 229-241.

Ministry of Housing and Urban-Rural Development of the People's Republic of China (MOHURD) (2012). "Technical specification for retaining and protection of building foundation excavations." *China Architecture & Building Press Beijing China*. (in Chinese)

PLAXIS *b.v.* (2002). *Plaxis program in 2 dimensions*, Version 8. *Netherlands*.

Shanghai Geology and Minerals Topology Editorial Board (SGMTEB) (1999). "Shanghai Geology and Minerals Topology (SGMT)." Shanghai Academy of Social Sciences Press Shanghai. (in Chinese)

Sun, Y. Y. and Zhou, S. H. (2011). "Discussion on yield criterions of soils on tensile-shear failure." *International Conference on Electric Technology and Civil Engineering*, pp. 2112-2115.

Taiwan Geotechnical Society (TGS) (2001). *Design specifications for the foundation of buildings*, TGS, Taipei, Taiwan.

Tanaka, T. and Verruijt, A. (1999). "Seepage failure of sand behind sheet piles: the mechanism and practical approach to analysis." *Soils and Foundations,* Vol. 39, No. 3, pp. 27-35.

Taylor, R. N. (1995). *Geotechnical centrifuge technology,* Blackie Academic and Professional London.

Terzaghi, K. (1943). *Theoretical soil mechanics*, New York Wiley.

Wang, C. D., Wang, B. L., Guo, P. J., and Zhou, S. H. (2015). "Experimental

analysis on settlement controlling of geogrid-reinforced pile-raft-supported embankments in high-speed railway." *Acta Geotechnica*, Vol. 10, No. 2, pp. 231-242, DOI: 10.1007/s11440-013-0288-6.

Wang, J. X., Feng, B., Guo, T. P., Wu, L. G., Lou, R. X., and Zhou, Z. (2013). "Using partial penetrating wells and curtains to lower the water level of confined aquifer of gravel." *Environmental Geology*, Vol. 161, No. 3, pp. 16-25, DOI: 10.1016 /j.enggeo.2013.04.007.

Wudtke, R. B. and Witt, K. J. (2006). "A static analysis of hydraulic heave in cohesive soil." *3rd International Conference on Scour and Erosion Amsterdam 1-3*, pp. 251-256.

Wudtke, R. B. (2008). "Failure mechanisms of hydraulic heave at excavation." *19th European Yong Geotechnical Engineers' Conference*, Gyor, Hungary.

Xu, Y. S., Shen, S. L., and Du, Y. J. (2009). "Geological and hydrogeological environment in Shanghai with geohazards to construction and maintenance of infrastructures." *Engineering Geology*, Vol. 109, No. 3, pp. 241-154, DOI: 10.1016/j.enggeo.2009.08.009.

Xu, Y. S., Shen, S. L., Du, Y. J., Chai, J. C., and Horpibulsuk, S. (2013). "Modeling the cutoff behavior of underground structure in multi-aquifer-aquitard groundwater system." *Nat Hazards*, Vol. 66, No. 12, pp. 731-748, DOI: 10.1007/s11069-012-0512-y.

Yin, Z. Z., Zhu, H., and Xu, G. H. (1995). "A study of deformation in the interface between soils and concrete." *Computers and Geotechnics*, Vol. 17, No. 1, pp. 75-92.

Zhang, X. S., Wang, J. X., Wong, H., Leo, C. J., Liu, Q., and Tand Y. Q. (2013). "Land subsidence caused by internal soil erosion owing to pumping confined aquifer groundwater during the deep foundation construction in Shanghai." *Nat Hazards*, Vol. 69, No. 13, pp. 718-725, DOI: 10.1007/s11069-013-0718-7.